

Atmospheric helium capillary dielectric barrier discharge for soft ionization: broadening of spectral lines, gas temperature and electron number density

Cite this: *J. Anal. At. Spectrom.*, 2014, 29, 498

Vlasta Horvatic,^a Saskia Müller,^b Damir Veza,^c Cedomil Vadla^a and Joachim Franzke^{*b}

The capillary helium dielectric barrier discharge (DBD) operating at atmospheric pressure was investigated by means of optical emission spectroscopy with the aim to determine the dominant broadening mechanism of the helium spectral lines, gas temperature and electron number density. The dependence of emission profiles of helium 388 nm, 501 nm, 587 nm, 667 nm, 706 nm and 728 nm lines on discharge voltage, helium pressure and position along the DBD capillary was investigated. Also, the pressure and voltage dependence of the profiles of hydrogen H-alpha and H-beta lines was examined. The Lorentzian widths of the normalized helium line profiles were found to be constant with respect to the applied voltage and the position along the capillary. The dominant broadening mechanism for all investigated lines was identified to be due to collisions with ground-state helium atoms, with the Stark broadening being negligible. It was determined that the temperature of the gas was constant along the capillary and independent of the voltage applied on the DBD electrodes and that its value coincided with the room temperature. The measurements of the dependence of the Lorentzian width of hydrogen H-alpha and H-beta lines on helium pressure, combined with gas temperature determined in the experiment, yielded the following values for the broadening parameters due to broadening by neutral helium: $\gamma_{\text{He}}^{\nu}(\text{H}_{\alpha}) = 1.56 \times 10^{-9} \text{ cm}^3 \text{ s}^{-1}$ and $\gamma_{\text{He}}^{\nu}(\text{H}_{\beta}) = 3.16 \times 10^{-9} \text{ cm}^3 \text{ s}^{-1}$. From the analysis of the measured H-alpha and H-beta line profiles the upper limit of the electron number density in the investigated plasma was obtained as $n_e \leq 1.4 \times 10^{12} \text{ cm}^{-3}$.

Received 18th October 2013
Accepted 14th November 2013

DOI: 10.1039/c3ja50343g

www.rsc.org/jaas

Introduction

In the last decade different types of plasmas were investigated to serve as ambient desorption ionization (ADI) sources for the detection and determination of molecular species.^{1–7} Applied soft ionization techniques (*e.g.*, as chemical ionization) as offered by ADI sources are attractive because they preserve the structural integrity of the molecules under study. Among others, the plasma jet produced by an atmospheric DBD was found to be a suitable source for soft ionization in ion mobility spectrometry (IMS) and mass spectrometry (MS).^{8–11}

In spite of numerous investigations dealing with the efficiency of helium DBDs as ambient ionization sources, the relevant ionization mechanisms leading to optimal enhancement of MS sensitivity are not ambiguously determined. First of all, the properties of the generated plasmas strongly depend on the construction and geometry of a particular DBD. Furthermore, for

a given construction geometry the plasma properties also strongly depend on the kind of electrodes, the gas flow and the applied voltage.

The study of He metastables (He^m) in the plasma is essential not only for better understanding of the mechanism by which helium-DBDs operate but also for the optimization of their performance for mass spectrometric analyses. It was also stated that Penning ionization from metastable helium is not the sole ionization pathway for the production of N_2^+ ions in the low temperature plasma (LTP) probe.¹² The importance of Penning ionization in the plasma of the dielectric barrier discharge or in the plasma jet was not refuted but it should be noted that He_2^+ ions could also play an important role in helium-plasma-based ionization sources.

The DBD can be operated in two different modes, homogeneous and filamentary modes. These modes can be distinguished by measuring the plasma current. Filamentary modes show multiple current peaks while a homogeneous mode has a well-defined current peak. The rotational temperature is constant along the discharge axis from the middle of the capillary to the positions in the jet where the N_2^+ 391 band is still measurable. In contrast to the homogeneous mode, in the filamentary mode there is a clear increase of rotational

^aInstitute of Physics, Bijenicka 46, 10000 Zagreb, Croatia

^bISAS—Leibniz Institut für analytische Wissenschaften, Bunsen-Kirchhoff-Str. 11, 44139 Dortmund, Germany. E-mail: franzke@isas.de

^cDepartment of Physics, Faculty of Science, University of Zagreb, Bijenicka 32, 10000 Zagreb, Croatia

temperatures when approaching the anode region and their values saturate in the jet at about 410 K.¹³

The aim of the present investigation is to identify the dominant broadening mechanism of the helium spectral lines, and to determine the gas temperature and estimate electron number density in the capillary barrier discharge. To this end the broadening of the helium and hydrogen lines in a DBD operating in the filamentary as well as in the homogeneous mode will be presented. The dependence of the line profiles on the applied voltage, helium pressure and the position along the discharge has been investigated, yielding important insight into the characteristics of the generated plasma.

Experiment and method

Experimental

The experimental arrangement is basically the same as reported in our previous works^{13,14} and it will be described here only briefly. The DBD was produced in a capillary quartz tube (length: 30 mm, outer diameter: 1 mm, inner diameter: 0.5 mm) with two electrodes (distance: 10 mm) in tight contact with the outer capillary surface. The discharge burned in He and was sustained by a homemade high-voltage generator with approximately sinusoidal output (frequency: 21.5 kHz, voltage amplitudes: up to 6.5 kV).

The emission signals were measured by a 1 m McPherson monochromator (grating: 1200 grooves per mm). The monochromator was supplied either with an RCA-S20 multiplier for measurements in the visible region or with an EMI S-11 multiplier for UV and visible regions. The photomultiplier current signals were measured by picoammeter (Keithley 4685) and stored in a laboratory PC. With our detection system, intensities of the spectral lines emitted within the period of time of plasma current duration (about 2 μ s) were averaged and recorded as continuous spectra. The spectra were obtained by scanning the monochromator, with the fastest scanning speed limited to 1 nm min⁻¹. This speed combined with the actual data acquisition rate was the highest scan speed at which adequate optical resolution of the recorded spectra was still maintained.

In the first part of the experiment, the measurements were performed at various helium flow rates at atmospheric pressure, provided by the same gas handling system as in our recent works.^{13,14} In contrast to that, a part of the present measurements was performed at helium pressures lower than 1 atmosphere. For this purpose the outlet side of the capillary was connected with a vacuum system as sketched in Fig. 1. The light emitted from the capillary discharge was imaged side-on by a lens (focal length: 10 cm) to the entrance slit of the monochromator. The quartz window of the vacuum chamber enabled the end-on measurements too.

Registered line intensities

The resulting spectral intensity of a line simultaneously emitted (2 \rightarrow 1) and absorbed (1 \rightarrow 2) in a plasma column (length L) is given by the expression (see, for instance Thorne *et al.*¹⁵)

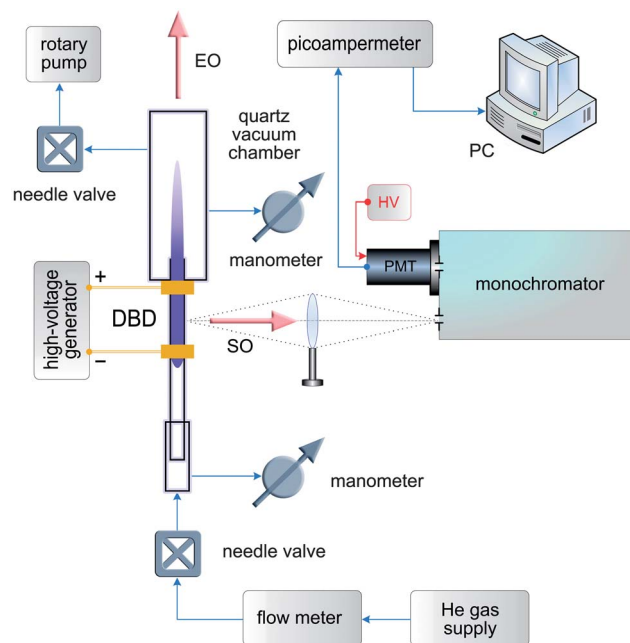


Fig. 1 The experimental arrangement. The arrows labeled with SO and EO indicate the side-on and end-on observation axes.

$$i_{21}(\Delta\nu) \propto \frac{8\pi h\nu_{21}^3}{c^3} \frac{n_2}{n_1} \frac{g_1}{g_2} \{1 - \exp[-k_{12}(\Delta\nu)L]\}, \quad (1)$$

where the frequency-dependent absorption coefficient is given by

$$k_{12}(\Delta\nu) = \frac{c^2}{8\pi\nu_{21}^2} n_1 \frac{g_2}{g_1} A_{21} P_n^{12}(\Delta\nu). \quad (2)$$

Here, $\Delta\nu = \nu - \nu_{21}$ is the frequency detuning from the line center, ν_{21} is the central line frequency (units: s⁻¹), n_1 and n_2 are the number densities (units: cm⁻³) of the atoms in the lower and upper states, respectively, g_1 and g_2 are the statistical weights, A_{21} is the radiative transition rate (units: s⁻¹) and $P_n^{12}(\Delta\nu)$ is frequency-dependent normalized ($\int P(\nu)d\nu = 1$) line profile (units: s⁻¹).

A registered spectral line intensity is a convolution of the emitted spectral intensity and the monochromator instrumental profile. The measurements were performed in the first as well as in the second order of grating dispersion with different monochromator slits (slit widths: 10 or 30 μ m). The widths of resulting instrumental profiles were at least 2 to 3 times smaller than the widths of the registered lines.

For the analysis of the line profiles it is important to prove that the absorption effects along the observation axis are negligible, *i.e.* that the emitted lines are optically thin. In the case of optically thin lines ($k_{12}L \ll 1$), expression (1) becomes

$$i_{21}(\nu)|_{\text{thin}} \propto h\nu_{21}n_2A_{21}P(\Delta\nu)L, \quad (3)$$

The optical thickness of the measured lines was controlled by comparison of the end-on and side-on measured line profiles, where the ratio of the effective plasma column lengths L_{EO} and L_{SO} , respectively, amounts to about 20. It was found out

that some of the end-on measured helium lines (388 nm, 501 nm, 587 nm and 667 nm) were absorbed between 20% and 70% in the line kernel. These values for maximum absorption imply that the corresponding line intensities measured side-on, *i.e.* with 20 times shorter optical paths, are optically thin. For the He 706 nm and 728 nm lines as well as for hydrogen lines (H-alpha and H-beta) the difference between side-on and end-on measured intensities was negligible. Thus it was justified that all side-on measured lines can be treated as optically thin.

The profiles of the measured lines

The broadening of the spectral lines under the present experimental conditions is expected to be governed by collisions of emitting atoms with the surrounding particles leading to homogeneous pressure broadening with Lorentzian profiles and non-homogeneous broadening by the Doppler effect with Gaussian profiles. The normalized Lorentzian profile can be written as

$$P_{21}^{nL}(\Delta\nu) = \frac{1}{2\pi} \frac{\Delta_L}{(\Delta_L/2)^2 + (\Delta\nu)^2} \quad (4)$$

where Δ_L (Hz) is the Lorentzian full width at half-maximum (FWHM), which is given as the product of perturber number density n_p and the impact broadening parameter γ_p^v ($\text{cm}^3 \text{s}^{-1}$). In the monoatomic medium, such as the investigated DBD burning in pure helium, the Lorentzian shape of helium lines is expected to be governed by collisions with neutral helium atoms and electrons. Then, the resulting Lorentzian FWHM is the sum of both contributions:

$$\Delta_L = \gamma_{\text{He}}^v n_{\text{He}} + \gamma_e^v n_e. \quad (5)$$

The normalized Doppler profile is a Gauss function given by:

$$P_{12}^{nD}(\nu) = \frac{2\sqrt{\ln 2}}{\sqrt{\pi}\Delta_D} \exp\left[-\left(\frac{\nu - \nu_{21}}{\Delta_D} 2\sqrt{\ln 2}\right)^2\right], \quad (6)$$

where $\Delta_D = (2\sqrt{\ln 2}/\lambda_{12})\sqrt{2kT/M}$ is the Doppler FWHM. Here, k , T and M label the Boltzmann constant, the gas temperature and the mass of an emitting particle, respectively.

In general, both Lorentz and Doppler broadening mechanisms are present and the resulting profiles are their convolutions, which are well known as the Voigt profiles. Finally, the registered signals $I_{21}(\nu)$ are given by the convolution of the instrumental profiles and the intrinsic Voigt profiles.

Determination of the Lorentzian line widths

The Lorentzian widths of the measured lines were determined from their wings, which is demonstrated here for the case of the He 667 nm line. In Fig. 2a the frequency-dependent intensity I_{667} of the He 667 line measured near the anode at atmospheric pressure is plotted together with the actual monochromator instrumental profile I_{IP} . This measurement was performed in the first order of the monochromator dispersion and the slits widths were 40 μm yielding the FWHM of the instrumental profile of 28 GHz at 667 nm.

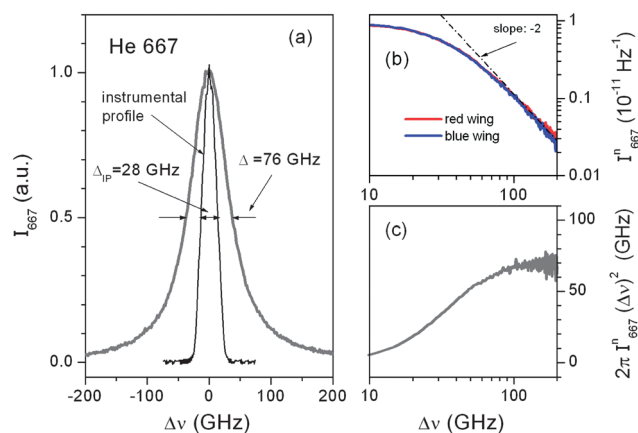


Fig. 2 An example for the determination of the Lorentzian FWHM from the line wings. In (a) part of the figure intensity is expressed in arbitrary units (a.u.). See further explanations in the text.

In general, in the line wings at detuning larger than 3 Doppler FWHMs, the Voigt profiles follow the shape of the Lorentzian component. Also, at detuning of about 3–4 FWHMs of the instrumental profile the registered line profile becomes directly proportional to the actual line profile. To get the insight in the present case, the normalized intensity $I_{667}^n = I_{667}/\int I_{667}d\nu$ was calculated and plotted in the double logarithmic scale in Fig. 2b.

Fig. 2a shows that at detuning of about $\Delta\nu = 100$ GHz the measured intensity of the He 667 line acquires a linear dependence on $(\Delta\nu)^2$ in the double logarithmic scale with a slope equal to -2 . This frequency dependence corresponds to the wings of the Lorentzian profile:

$$I_{667}^n \equiv P_{21}^{nL}(\Delta\nu) = \frac{1}{2\pi} \frac{\Delta_L}{(\Delta\nu)^2} \quad (\Delta\nu)^2 \gg (\Delta_L/2)^2 \quad (7)$$

which can be used to determine the Lorentzian line width. The averaged values for $\Delta_L = 2\pi I_{667}^n (\Delta\nu)^2$ obtained from the red and blue wings of the I_{667}^n profile are plotted in Fig. 2c. In the present example, the data saturate at $\Delta\nu > 100$ GHz and yield the value $\Delta_L \approx 68$ GHz.

Broadening of helium lines

The characteristic parameters of six helium lines measured here are listed in Table 1. The lines are related to the four lowest excited states of helium, which include an excited state $2p^3P^o_J$, two metastable states ($2s^3S_1$ and $2s^1S$), and the first resonance

Table 1 Basic data for the investigated helium spectral lines¹⁶

λ (nm)	Transition	E_i (cm^{-1})	E_k (cm^{-1})	g_i	g_k	A_{ki} (10^8 s^{-1})
388.8	$2s^3S_1-3p^3P^o_J$	159 856	185 565	3	9	0.095
501.5	$2s^1S-3p^1P^o$	166 278	186 210	1	3	0.13
587.6	$2p^3P^o_J-3p^3D_J$	169 087	186 102	9	15	0.71
667.8	$2p^1P^o-3d^1D$	171 135	186 105	3	5	0.638
706.5	$2p^3P^o_J-3s^3S_1$	169 087	183 237	9	3	0.278
728.1	$2p^1P^o-3s^1S$	171 135	184 865	3	1	0.18

($2p\ ^1P^o$) state. Some of these lines are singlets (501 nm, 667 nm, 728 nm), while others exhibit fine structures. The tabulated parameters for 388 nm, 587 nm and 706 nm lines are related to overall multiplet values.¹⁶

The frequency distances and relative intensities of the fine-structure components of investigated helium multiplet lines are listed in Table 2. Here the data taken from NIST¹⁷ were used. The frequency distances Δ_{FS} are expressed relative to the position of the strongest component of the particular multiplet.

As mentioned before, in the plasma generated inside the capillary DBD, the helium lines are expected to be broadened by collisions with neutral helium atoms and electrons, and the line widths defined by eqn (5) reflect this. To investigate the influence of physical conditions in the DBD on the line profiles, for each of the six measured helium lines the experiments were performed by changing the particular discharge parameter. In the following, the detailed results will be presented for the case of He 706 nm and He 587 nm lines.

The He line profiles depending on the applied voltage, the position along the capillary and the helium pressure

The measurements of the He line profile dependence on the discharge voltage as well as on the position along the capillary were performed at the gas flow rate of $500\ \text{ml}\ \text{min}^{-1}$ and the plasma jet penetrated in the ambient air atmosphere. The capillary DBD was observed side-on in the region near the anode. The voltage was varied between 3.5 kV and 6.5 kV. At 3.5 and 4.0 kV the DBD operated in the homogeneous mode, while at the higher voltages it operated in the filamentary mode. The results obtained for the He 706 nm line are presented in Fig. 3.

These measurements were performed in the first order of grating dispersion with $10\ \mu\text{m}$ wide monochromator slits, which yielded a FWHM of the instrumental profile of about 7 GHz at 706 nm. As can be seen in Fig. 3a, the profiles of the measured He 706 nm line are slightly asymmetric in the line kernel which is due to the fine-structure component at $\Delta_{FS} = -31.8\ \text{GHz}$. This becomes more apparent in Fig. 3b where the normalized intensities are plotted in the double logarithmic scale. The measured line intensities strongly depend on the discharge voltage. However, the normalized line intensities

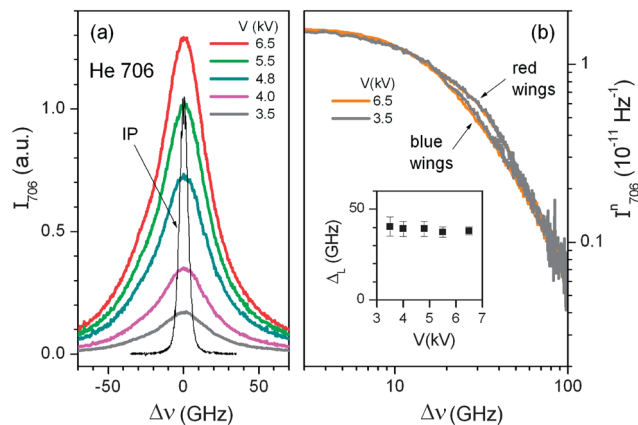


Fig. 3 The profiles of the He 706 nm line measured side-on at the position near the anode at atmospheric pressure and the constant helium flow, while the applied voltage was changed. IP labels the instrumental profile. (a) Measured signals obtained at various discharge voltages. (b) Red and blue wings of the normalized profiles obtained at lowest and highest voltages and plotted in the double logarithmic scale. The inset in (b) displays evaluated Lorentzian widths depending on the applied voltage.

exhibit the same Lorentzian shape in the wings and the evaluated Lorentzian widths ($\Delta_L = 39\ \text{GHz}$) were found to be independent of the DBD-voltage within the experimental error bars ($\pm 10\%$). The Lorentzian widths of the other investigated helium lines were also found to be independent of the applied voltage.

As mentioned previously, contributions to the Lorentzian width are due to collisions with neutral He atoms and electrons by Stark broadening. If Stark broadening is appreciable it would certainly reflect itself in the noticeable change of the Lorentzian width by alteration of the DBD operating voltage. The constancy of Δ_L with respect to the applied voltage leads to the conclusion that helium lines under the conditions of the investigated DBD do not depend on the electron density and that the broadening is dominantly caused by collisions with neutral helium atoms.

The side-on measured intensities of helium lines were found to be strongly dependent on the observation position x along the capillary. This was especially pronounced in the filamentary mode at the highest voltages, as a consequence of the nonhomogeneous electron number density distribution. However, the line profiles, *i.e.* their Lorentzian widths, remained unchanged. Fig. 4 shows the results obtained for the He 706 nm line. The side-on intensities were measured in the middle of the capillary and at two positions near the anode (see Fig. 4), while the discharge voltage was kept constant. The evaluated Lorentzian FWHMs obtained in this part of the measurement are fully in agreement with the values obtained at various voltages.

It should be stressed that at higher applied gas flows the Lorentzian widths of the helium lines slightly increase. For instance, when increasing the gas flow to $1.5\ \text{l}\ \text{min}^{-1}$, the values of Δ_L are about 5–10% higher than those at the flow of $500\ \text{ml}\ \text{min}^{-1}$. This effect is obviously due to an increase of the helium pressure in the capillary at higher gas flows. To examine the pressure dependence of the helium line broadening parameters the following set of measurements was performed.

Table 2 Basic data for the structure of the investigated helium multiplet lines¹⁷

λ (nm)	Transition	Δ_{FS} (GHz)	Relative intensity
388.8	$2s\ ^3S_1-3p\ ^3P^o_2$	0	0.555
	$-3p\ ^3P^o_1$	+0.66	0.333
	$-3p\ ^3P^o_0$	+9.44	0.112
587.6	$2p\ ^3P^o_2-3p\ ^3D_1$	+1.41	0.005
	$-3p\ ^3D_2$	+0.06	0.083
	$-3p\ ^3D_3$	0	0.469
	$2p\ ^3P^o_1-3p\ ^3D_1$	-0.87	0.083
	$-3p\ ^3D_2$	-2.22	0.25
706.5	$2p\ ^3P^o_0-3p\ ^3D_1$	-30.5	0.11
	$2p\ ^3P^o_2-3s\ ^3S_1$	0	0.555
	$-2p\ ^3P^o_1$	-2.1	0.333
	$-2p\ ^3P^o_0$	-31.8	0.112

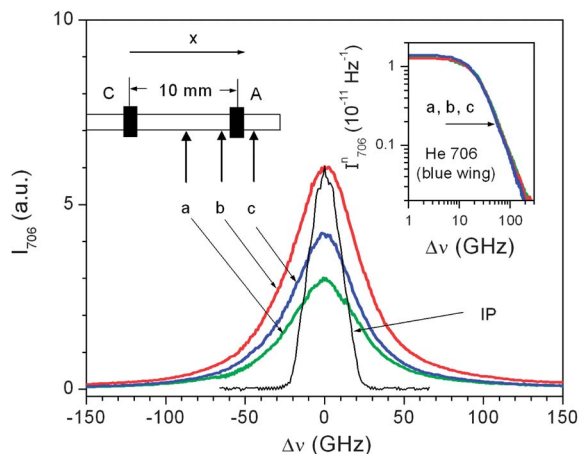


Fig. 4 The profiles of the He 706 nm line measured side-on at various x -positions (a–c). The DBD operating voltage and He flow were kept constant at 5.6 kV and 500 ml min⁻¹, respectively. In the present case the width of the monochromator slits was 40 μ m and the FWHM of the corresponding instrumental profile (IP) is about 25 GHz. The inset on the right side: blue wings of the normalized profiles plotted in the double logarithmic scale.

The gas-outlet side of the capillary was connected to the vacuum system and the pressure in the chamber and the capillary was controlled by needle valves (see Fig. 1). The measurements were performed keeping the gas flow under standard conditions in the range between 200 and 500 ml min⁻¹ while the pressure was varied from 1200 mbar down to approximately 400 mbar. As an example of the pressure dependence of the investigated He lines, the results of the profiles of the He 587 nm line are shown in Fig. 5. The applied voltage was 6.5 kV and the discharge was observed side-on at the position near the anode.

The evaluated Lorentzian width Δ_L at atmospheric pressure amounts to (34 ± 5) GHz and exhibits a clear linear dependence while changing the pressure. The slope of the linear fit through the data plotted in the inset of Fig. 5b amounts to 0.036 GHz mbar⁻¹. Within the error bar (± 5 GHz), the extrapolated value of the Lorentzian FWHM for the zero pressure equals zero. This again corroborates the finding that the Stark broadening of helium lines under the present experimental conditions is negligible.

Lorentzian widths of the helium lines and the determination of the gas temperature

The performed investigation of the helium line profiles observed side-on from the capillary DBD burning in pure helium at atmospheric pressure shows that the line wings of all measured lines are basically of the Lorentzian type. Within the error bars, the measured Lorentzian widths are independent of the discharge voltage and, at lower gas flows, independent of the position of observation along the discharge axis. The Lorentzian widths Δ_L^{atm} of the helium lines measured here at atmospheric pressure are listed in Table 3.

The broadening of helium spectral lines due to collisions with ground state helium atoms has been the subject of many experimental and theoretical investigations with the goal to

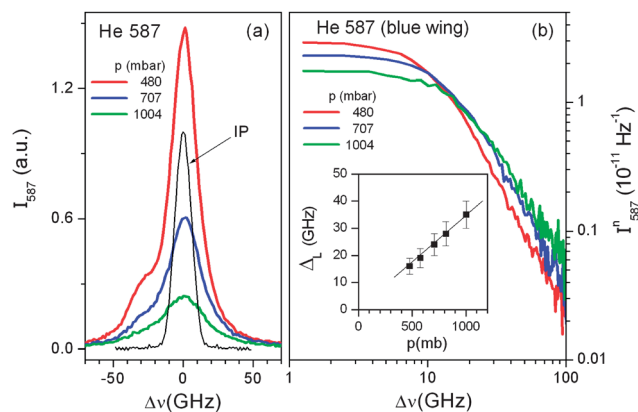


Fig. 5 (a) The intensities of the He 587 nm line measured at three different helium pressures with an applied voltage of 6.5 kV. With decreasing pressure the hyperfine component at $\Delta_{FS} = -30.5$ GHz becomes more pronounced. The measurements were done in the second order of grating dispersion with the monochromator slits widths of 40 μ m. The instrumental profile (IP) for that case is represented by the grey line. (b) Blue wings of the normalized profiles in the double logarithmic scale. The inset in (b) shows the evaluated Lorentzian widths depending on helium pressure obtained from the presented profiles and two additional ones which are not shown here.

obtain information about the mechanisms of relevant inter-atomic interactions during the collisions. As reported in the literature^{18–23} for the lines investigated here, the main mechanisms of this broadening are van der Waals and resonance interactions. The transitions at 501.5 nm, 667.8 nm and 728.1 nm are influenced by resonance interactions, whereas the other three transitions (at 388.8, 587.6 and 706.5 nm) are broadened purely by van der Waals interaction.

The data for the impact broadening parameters γ_{He}^{ν} taken from the literature at our disposal are listed in Table 4. According to the theory, the impact broadening parameters due to pure van der Waals interactions are dependent on the gas temperature ($\propto T_g^{0.3}$) and the data listed in Table 4 were obtained at temperatures between 273 and 300 K. In the case of pure resonance interactions the broadening parameters are temperature-independent.

Similarly, as shown for the case of the He 587 nm line, the Lorentzian widths of all measured lines exhibit a clear linear dependence on the helium pressure with residual values $0 < \Delta_L^{\text{res}} < 5$ GHz, which can be attributed to the small Stark contributions $n_e \gamma_e^{\nu}$. Thus, in the present case, the relationship (5) reduces to $\Delta_L^{\text{atm}} \approx \Delta_{\text{vdW}}^{\text{atm}} = n_{\text{He}}^{\text{atm}} \gamma_{\text{He}}^{\nu}$, which combined with the

Table 3 Lorentzian widths Δ_L^{atm} measured at atmospheric pressure

He line (nm)	Δ_L^{atm} (GHz)
728	61 \pm 5
706	39 \pm 4
667	68 \pm 4
587	35 \pm 4
501	44 \pm 4
388	39 \pm 7

Table 4 The literature values of the self-broadening parameters γ_{He}^{ν} of the investigated lines, the corresponding dominant broadening mechanism (vdW – van der Waals interaction, R – resonance interaction) and the gas temperatures T_g obtained in the present experiment. See further explanations in the text

He line (nm)	γ_{He}^{ν} ($10^{-9} \text{ cm}^3 \text{ s}^{-1}$)	Method	Dominant broadening mechanism	Reference	T_g (K)
728	2.86	Exp.	R	18	339
	1.98	Theory		19	(235)
706	1.37	Exp.	vdW	20	254
	1.72	Theory		21	319
	1.63	Theory		22	303
667	2.49	Exp.	R	18	265
	2.64, 2.97	Exp.		23	281, 316
	1.21	Theory		19	(129)
587	0.9	Exp.	vdW	24	(186)
	1.3	Theory		21	269
501	6.03	Exp.	vdW > R	18	(993)
	1.66	Theory		19	273
388	1.57	Theory	vdW	21	291
	1.45	Theory		22	269

broadening parameter data for γ_{He}^{ν} listed in Table 4 enables determination of the number density $n_{\text{He}}^{\text{atm}}$ of helium ground-state atoms at atmospheric pressure and subsequently the gas temperature by applying Dalton's law. Using the data given in Tables 3 and 4 the values of $T_g = \gamma_{\text{He}}^{\nu} p / \Delta_{\text{vdW}}^{\text{atm}} k$ were calculated and are listed in the last column of Table 4. Here, p and k are the pressure and the Boltzmann constant, respectively. As can be seen in Table 4, four obtained values for T_g strongly deviate from the rest of the calculated dataset. These values, given in brackets, were omitted in the performed statistics as highly unlikely candidates for the correct gas temperature. The remaining eleven values yield the most probable value $T_g = 290$ K, with the statistical accuracy of about 10%. If the upper limit of 5 GHz corresponding to the Stark broadening contribution is taken into account, the resulting values for $\Delta_{\text{vdW}}^{\text{atm}}$ are lower, which consequently increases the most probable gas temperature by ~ 30 K, *i.e.* to 320 K.

In many publications, the gas temperature of an atmospheric DBD is assumed and widely accepted to be near the room temperature. This assumption has been based on several side effects that led to the conclusion that the atmospheric DBD plasma is a cold plasma. To the best of our knowledge, the present work represents the first spectroscopic confirmation of this statement.

Hydrogen lines

In the course of the present experiment, the hydrogen lines at 656.3 nm (H-alpha) and 486.2 nm (H-beta) were examined too. The objective of these measurements was to get information about actual electron density in our capillary DBD. The Stark impact broadening of these hydrogen lines is well known and they are often used as reliable standards for the determination of the electron number density in ionized gases. In contrast to

helium lines, side-on signals of hydrogen lines were very weak, and therefore these lines were measured end-on so that their intensities are related to the whole discharge volume. Both lines were measured as functions of the helium pressure in the filamentary operating mode of the DBD at $V = 6.5$ kV. Typical spectra and corresponding normalized intensities are plotted in Fig. 6. In addition, the H-beta line was measured at a lower voltage ($V = 4.2$ kV) in the homogeneous discharge mode. Both lines are multiplets, but their fine-structure splitting is smaller than the widths of the instrumental profiles involved.

The broadening parameter Δ_L obtained from the Lorentzian wings of the normalized line intensities are depicted in Fig. 7.

The present measurement shows that the hydrogen lines exhibit a behavior similar to the helium lines. Hydrogen number density in the capillary is negligible in comparison with the density of helium, so that the pressure broadening of hydrogen lines is essentially due to helium ground state atoms. The slopes of the linear fits through the data plotted in Fig. 7 amount to $0.079 \text{ GHz mbar}^{-1}$ and $0.039 \text{ GHz mbar}^{-1}$ for the H-beta and H-alpha lines, respectively. Within the error bar (± 3 GHz), the extrapolated values of the Lorentzian FWHM are equal to zero for the zero pressure. By taking into account the value $T_g = 290$ K, the data presented in Fig. 7 yield the broadening parameters $\gamma_{\text{He}}^{\nu}(\text{H}_{\alpha}) = 1.56 \times 10^{-9} \text{ cm}^3 \text{ s}^{-1}$ and $\gamma_{\text{He}}^{\nu}(\text{H}_{\beta}) = 3.16 \times 10^{-9} \text{ cm}^3 \text{ s}^{-1}$. There are two results available in the literature for $\gamma_{\text{He}}^{\nu}(\text{H}_{\alpha})$. Kielkopf²⁵ reported the value of the integral broadening of the blended H-alpha line of $1.44 \times 10^{-9} \text{ cm}^3 \text{ s}^{-1}$ measured at 800 K. Weber²⁶ made the measurements of the resolved H-alpha fine-structure lines at 310 K, and obtained broadening constants for the particular components in the range between $1.44 \times 10^{-9} \text{ cm}^3 \text{ s}^{-1}$ and $2.04 \times 10^{-9} \text{ cm}^3 \text{ s}^{-1}$. All mentioned results are in very good agreement with the $\gamma_{\text{He}}^{\nu}(\text{H}_{\alpha})$ value obtained in the present investigation. To the best of our knowledge $\gamma_{\text{He}}^{\nu}(\text{H}_{\beta})$ has not been measured yet, and the present

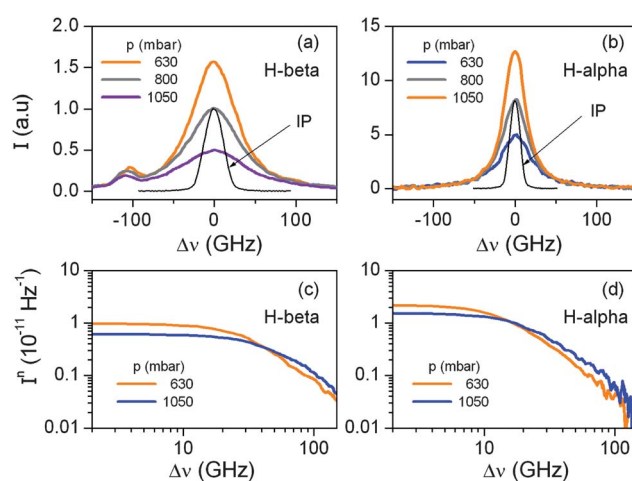


Fig. 6 (a) The H-beta line profiles measured end-on at various helium pressures in the DBD. The feature in the red wing of H-beta is an unidentified molecular transition. (b) The same as in (a) but for the H-alpha line. Both measurements were performed at $V = 6.5$ kV. (c) The intensity of the blue wing of the normalized line profile of the H-beta line in the double-logarithmic scale. (d) The same as in (c) but for the H-alpha line.

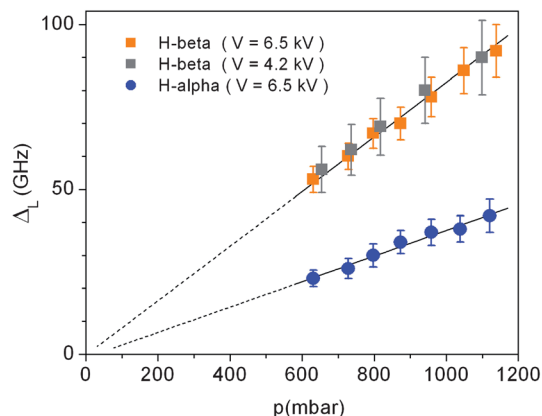


Fig. 7 The evaluated Lorentzian line widths of the H-alpha and H-beta lines depending on helium pressure measured in a filamentary DBD mode ($V = 6.5$ kV) with residual values $\Delta_{L,\beta}^{\text{Stark}}$ indicated for helium zero-pressure. In addition, the data for the H-beta line obtained at 4.2 kV (homogeneous mode) are plotted.

value represents the first experimental result for this broadening parameter. However, according to recent theoretical estimation²⁷ the mean van der Waals broadening of the H-beta line due to helium at 1 atm and 300 K was reported to be 44.6 pm (56 GHz). The corresponding value for $\gamma_{\text{He}}^{\nu}(\text{H}_{\beta})$ is lower than that measured here and amounts to $2.31 \times 10^{-9} \text{ cm}^3 \text{ s}^{-1}$.

The Stark contribution to the impact broadening of the hydrogen lines is negligible and only a rough estimation of the maximum electron number density can be made. The Stark widths are complex functions of electron density and electron temperature.²⁸ However, according to Gigosos *et al.*²⁹ in a wide range of electron temperatures (up to 10 000 K) simple relationships for Stark contributions to the Lorentzian widths of the hydrogen lines can be used for determination of electron number density. In the case of H-beta lines the following expression can be applied:

$$\Delta_{L,\beta}^{\text{Stark}} (\text{nm}) = 4.60 \times [10^{-17} \times n_e (\text{cm}^{-3})]^{0.681} \quad (8)$$

As mentioned above, the upper value of the Stark contribution $\Delta_{L,\beta}^{\text{Stark}}$ to the Lorentzian width is estimated to be 3 GHz. From eqn (8) it follows that in the investigated DBD electron number density was $n_e \leq 1.4 \times 10^{12} \text{ cm}^{-3}$.

Conclusions

The capillary DBD operating in helium at atmospheric pressure was investigated by means of optical emission spectroscopy in a series of experiments with the aim to perform the diagnostics of the generated plasma. The emission profiles of helium 388 nm, 501 nm, 587 nm, 667 nm, 706 nm and 728 nm lines were investigated as functions of the discharge voltage (in the range 3.5–6.5 kV), helium pressure (in the range 500–1000 mbar) and position along the DBD capillary. In addition, the dependence on the helium pressure of the profiles of hydrogen H-alpha and H-beta lines was measured. In the case of the H-beta line the dependence on the applied voltage was inspected too.

The measured total intensities of helium lines strongly depend on voltage and position of observation, which is due to the pronounced non-homogeneity of the plasma regarding the electron concentration and electron-impact excitation. However, the analysis of the normalized line profiles showed that their Lorentzian widths do not depend either on the applied voltage or the position along the capillary, and that line shapes are dominantly governed by impact broadening due to collisions with ground-state helium atoms. The contribution from Stark broadening was found to be negligible in comparison with the van der Waals broadening due to interactions with helium ground-state atoms, even at highest applied voltages. From the measured Lorentzian widths and the data for the line broadening parameters from the literature, the gas temperature was determined. Its value, which is constant along the capillary axis and independent of the voltage applied on the DBD electrodes, was found to coincide with the room temperature within the experimental error bar.

The hydrogen H-alpha and H-beta lines exhibited a behavior similar to the helium lines. Under the present conditions in the DBD they are dominantly broadened by collisions with helium ground state atoms, which is plausible bearing in mind that in the capillary the hydrogen is present in traces. From the measurements of the gas temperature and the Lorentzian widths of these lines vs. He pressure the broadening parameters $\gamma_{\text{He}}^{\nu}(\text{H}_{\alpha}) = 1.56 \times 10^{-9} \text{ cm}^3 \text{ s}^{-1}$ and $\gamma_{\text{He}}^{\nu}(\text{H}_{\beta}) = 3.16 \times 10^{-9} \text{ cm}^3 \text{ s}^{-1}$ were obtained. To the best of our knowledge this is the first experimental result for H-beta broadening by neutral helium, and the value is in reasonable agreement with the theoretical value²⁵ of $2.31 \times 10^{-9} \text{ cm}^3 \text{ s}^{-1}$. In the present experiment only an upper limit of the electron number density could be determined and it amounted to $n_e \leq 1.4 \times 10^{12} \text{ cm}^{-3}$.

Our further interest lies in the determination of the number densities in the helium metastable states by means of the emission spectroscopy. To apply this method reliably, accurate information about the profiles of the relevant spectral lines as well as the basic plasma parameters is needed. The helium lines investigated here emerge in the transitions related to the four lowest helium excited states including two metastable states, and supply necessary information for the application of the mentioned method.

The findings that in the helium capillary DBD the helium lines are dominantly broadened due to collisions with ground state He atoms, with Stark broadening being negligible, that this broadening is independent of the discharge voltage and the position along the capillary, and that the gas temperature is equal to room temperature are very important because they simplify significantly the evaluation of number densities of interest from the emission intensities which have undergone simultaneous emission and absorption in the medium.

Acknowledgements

Financial support by the Ministerium für Innovation, Wissenschaft und Forschung des Landes Nordrhein-Westfalen, the Bundesministerium für Bildung und Forschung, the Deutsche Forschungsgemeinschaft (project no. FR 1192/13-1) and the Ministry of Science, Education and Sports of the Republic of Croatia (project no. 035-0352851-2853) is gratefully acknowledged.

References

- 1 N. Na, M. Zhao, S. Zhang, C. Yang and X. Zhang, *J. Am. Soc. Mass Spectrom.*, 2007, **18**, 1859–1862.
- 2 J. D. Harper, N. A. Charipar, C. C. Mulligan, X. Zhang, R. G. Cooks and Z. Ouyang, *Anal. Chem.*, 2008, **80**, 9097–9104.
- 3 J. S. Wiley, J. F. Garcia-Reyes, J. D. Harper, N. A. Charipar, Z. Ouyang and R. G. Cooks, *Analyst*, 2010, **135**, 971–979.
- 4 A. U. Jackson, T. Shum, E. Sokol, A. Dill and R. G. Cooks, *Anal. Bioanal. Chem.*, 2011, **399**, 367–376.
- 5 M. Z. Huang, S. S. Jhang, C. N. Cheng, S. C. Cheng and J. Shiea, *Analyst*, 2010, **135**, 759–766.
- 6 Y. Zhang, X. X. Ma, S. C. Zhang, C. D. Yang, Z. Ouyang and X. R. Zhang, *Analyst*, 2009, **134**, 176–181.
- 7 Y. Y. Liu, Z. Q. Lin, S. C. Zhang, C. D. Yang and X. R. Zhang, *Anal. Bioanal. Chem.*, 2009, **395**, 591–599.
- 8 A. Michels, S. Tombrink, W. Vautz, M. Miclea and J. Franzke, *Spectrochim. Acta, Part B*, 2007, **62**, 1208–1215.
- 9 W. Vautz, A. Michels and J. Franzke, *Anal. Bioanal. Chem.*, 2008, **391**, 2609–2615.
- 10 S. B. Olenici-Craciunescu, A. Michels, C. Meyer, R. Heming, S. Tombrink, W. Vautz and J. Franzke, *Spectrochim. Acta, Part B*, 2009, **64**, 1253–1258.
- 11 H. Hayen, A. Michels and J. Franzke, *Anal. Chem.*, 2009, **81**, 10239–10245.
- 12 G. C. Y. Chan, J. T. Shelley, J. S. Wiley, C. Engelhard, A. U. Jackson, R. G. Cooks and G. M. Hieftje, *Anal. Chem.*, 2009, **83**, 3675–3686.
- 13 S. Müller, T. Krähling, D. Veza, V. Horvatic, C. Vadla and J. Franzke, *Spectrochim. Acta, Part B*, 2013, **85**, 104–111.
- 14 S. B. Olenici-Craciunescu, S. Müller, A. Michels, V. Horvatic, C. Vadla and J. Franzke, *Spectrochim. Acta, Part B*, 2011, **66**, 268–273.
- 15 A. Thorne, U. Litzén and S. Johanson, *Spectrophysics – Principles and Applications*, Springer Verlag, Berlin–New York–Tokio, 1999.
- 16 W. L. Wiese, M. W. Smith and B. M. Glennon, *Atomic transition Probabilities*, National Standard Reference data Series, U.S. Government Printing Office, Washington D. C., 1966, vol. 1.
- 17 <http://physics.nist.gov>.
- 18 A. Atiola, B. C. Gibson-Wilde, A. C. Lindsay, J. L. Nicol and I. B. Whittingham, *J. Phys. B: At., Mol. Opt. Phys.*, 1988, **21**, 249–257.
- 19 D. F. T. Mullaamphy, G. Peach and I. B. Whittingham, *J. Phys. B: At., Mol. Opt. Phys.*, 1991, **24**, 3709–3726.
- 20 J. F. Su and J. L. Nicol, *J. Phys. B: At., Mol. Opt. Phys.*, 1990, **23**, 2215–2222.
- 21 P. J. Leo, D. F. T. Mullaamphy, G. Peach and I. B. Whittingham, *J. Phys. B: At., Mol. Opt. Phys.*, 1992, **25**, 1161–1173.
- 22 P. J. Leo, G. Peach and I. B. Whittingham, *J. Phys. B: At., Mol. Opt. Phys.*, 1995, **28**, 591–607.
- 23 A. C. Lindsay, J. L. Nicol, D. N. Stacey and P. E. Baird, *J. Phys. B: At., Mol. Opt. Phys.*, 1989, **22**, L303–L307.
- 24 J. Röhe-Hansen, K. Jeß and V. Helbig, *J. Phys. B: At., Mol. Opt. Phys.*, 1987, **20**, 4993–5003.
- 25 J. F. Kielkopf, *J. Chem. Phys.*, 1975, **62**, 3784–3787.
- 26 E. W. Weber, *Phys. Rev. A: At., Mol., Opt. Phys.*, 1979, **20**, 2278–2286.
- 27 G. C.-Y. Chan, J. T. Shelly, A. U. Jackson, J. S. Wiley, C. Engelhard, R. G. Cooks and G. M. Hieftje, *J. Anal. At. Spectrom.*, 2011, **26**, 1434–1444.
- 28 H. R. Griem, *Principles of Plasma Spectroscopy*, Cambridge University Press, 1997.
- 29 M. A. Gigosos, M. A. Gonzalez and V. Cardenoso, *Spectrochim. Acta, Part B*, 2003, **58**, 1489–1504.